Eur. Phys. J. E (2011) **34**: 9
DOI 10.1140/epje/i2011-11009-8

THE EUROPEAN PHYSICAL JOURNAL E

Regular Article

Free-standing urethane/urea elastomer films undoped and doped with ferro-nano-particles

C. Sena[1,a], M.H. Godinho[2,b], P.J. Sebastião[3,4,c], D. Sousa[5,d], and A.M. Figueiredo Neto[1,e]

[1] Instituto de Física, Universidade de São Paulo, caixa postal 66318, 05314-970, São Paulo, São Paulo, Brazil
[2] Faculdade de Ciências e Tecnologia e CENIMAT/I3N, Universidade Nova de Lisboa, Quinta da Torre, P-2829-519 Caparica, Portugal
[3] Centro de Física da Matéria Condensada, Av. Prof. Gama Pinto 2, 1649-003, Lisboa, Portugal
[4] Departamento de Física, Instituto Superior Técnico, TU Lisbon, Av. Rovisco Pais 1, 1049-001 Lisboa, Portugal
[5] DEEC AC-Energia, Instituto Superior Técnico, TU Lisbon, Av. Rovisco Pais 1, 1049-001, Lisboa, Portugal

Received 16 August 2010 and Received in final form 19 October 2010
Published online: 24 January 2011 –

Abstract. We report on an experimental study of the structures presented by urethane/urea elastomeric films without and with ferromagnetic nanoparticles incorporated. The study is made by using the X-ray diffraction, nuclear magnetic resonance (NMR), optical, atomic and magnetic force (MFM) microscopy techniques, and mechanical assays. The structure of the elastomeric matrix is characterized by a distance of 0.46 nm between neighboring molecular segments, almost independent on the stretching applied. The shear casting performed in order to obtain the elastomeric films tends to orient the molecules parallel to the flow direction thus introducing anisotropy in the molecular network which is reflected on the values obtained for the orientational order parameter and its increase for the stretched films. In the case of nanoparticles-doped samples, the structure remains nearly unchanged although the local order parameter is clearly larger for the undoped films. NMR experiments evidence modifications in the molecular network local ordering. Micrometer size clusters were observed by MFM for even small concentration of magnetic particles.

1 Introduction

In 1999, Zhao and Pinho [1] proposed an elegant method to prepare elastomers for pervaporation membranes, from polypropylene oxide isocianate terminated triol prepolymer (PU) and polybutadiene diol (PBDO). The crosslink reactions depend on the relative amount of PU and PBDO generating urethane/urea networks [1]. This type of material was shown to present different degrees of phase separation, depending on the relative concentrations of both pre-polymers [2].

Free-standing films produced from these materials were found to present interesting optical and mechanical properties [3,4]. Stress-induced birefringence [5–7] and also textures were identified on the surface of PU/PBDO films, with periodicities varying from about $3\,\mu$m to $10\,\mu$m [8]. Godinho and co-workers [3] used small-angle light scattering technique to investigate the bulk structure of these elastomers in the length scale of μm, and described the mechanic-optical induced patterns formation in thin films with and without UV light exposure. The use of PU/PBDO elastomers have been reported for lithography purposes [4] and as scaffolds for tissue engineering [4].

Nuclear magnetic resonance experiments performed with PU/PBDO elastomers [9] revealed that the proton spin-lattice relaxation time dispersion measured is typical of a molten chain dynamics. In this molecular length scale, the results obtained with these barely isotropic elastomers (since the casting could introduce a small anisotropy on them during the film preparation) were similar to those obtained from isotropic polymer networks.

Another smart material based on elastomers is the ferrogel, which is constituted by ferromagnetic nano [10] or microparticles [11] embedded in the elastomeric matrix. By the action of magnetic field and field gradients, ferrogels show an elongation and contraction behavior [12,13]. It was shown that a permanent optical anisotropy can be induced when applying a magnetic field during the sol-gel freezing process [14]. The mechanic-magneto-optical properties of these materials lead to many different applications, from soft actuators or micromanipulators in

[a] e-mail: cleidios@if.usp.br
[b] e-mail: mhg@fct.unl.pt
[c] e-mail: pedro.jose.sebastiao@ist.utl.pt
[d] e-mail: duarte.sousa@ist.utl.pt
[e] e-mail: afigueiredo@if.usp.br

technical fields, to applications in medicine, where they might act as artificial muscles or carriers for drugs [1, 15,16]. Recently, Suthar and co-workers [17] reported on the characterization of ferrogels with γ-Fe_2O_3 and Fe_3O_4 nanoparticles by using transmission electron microscopy and ultra-small-angle X-ray scattering. Their analysis focused on the nanoparticles agglomeration characteristics in the process of elastomer synthesis. Lebedev and co-workers [18] reported on neutron scattering results of ferrogels under applied magnetic field. They also verified the formation of particles' agglomerates due to the field. Since these authors focused on the magnetic particles ordering, an eventual modification of the elastomeric matrix by the presence of the nanoparticles was not reported. An important aspect to be stressed is that the relative weight concentration (wt.%) of magnetic particles in ferrogels may vary from about 2 wt.% [10] until about 30 wt.% [11] of magnetic content. Ashjari *et al.* [19] reported a study where magnetite nanoparticles were homogeneously dispersed in the PU matrix after tetrahydrofuran casting. The resulting nanostructured material presented interesting mechanical properties as, for example, modification of its toughness. Recently Sánchez-Ferrer *et al.* [20] reported an interesting study about the synthesis of inorganic-organic elastomer nanocomposite with integrated ellipsoidal silica-coated hematite spindle-type nanoparticles. These nanoparticles act as crosslinking agents within the elastomeric matrix. Modifications in the nanoparticles transform them in crosslinkable agents, modifying the composite properties.

One could expect that the macroscopic properties of the elastomers and ferrogels are influenced by their nanometric structure and local ordering. In the case of the elastomers we have the molecular network and, in the case of ferrogels, the molecular network and the nanoparticles incrusted on it. Structural information is important not only from the fundamental point of view but also for eventual applications [21]. In this paper we report on X-ray diffraction, nuclear magnetic resonance, optical, atomic and magnetic force microscopy and mechanical assays performed with PU/PBDO elastomers and ferrogels thin free-standing films. In the case of ferrogels, we focus particularly on the behavior of the diluted regime, where the concentration of magnetic material in the samples is less than 0.4 wt.%. We expect to investigate the early modifications on the elastomers' structure and behavior perturbed by the presence of just a small quantity of magnetic material. Moreover, when the magnetic material concentration is higher, some experimental methods used in the present study (*e.g.*, NMR) could not be employed because the material fingerprint signal becomes too weak to be detected due to the presence of magnetic nanoparticles. The experiments were performed with samples unstretched and, in some cases, subjected to a mechanical uniaxial stress. The Young moduli, stress and strain at break and the toughness of the different samples were measured and the results discussed in the framework of the proposed structure. Those mechanical properties were correlated to the development and relaxation of patterns in UV irradiated samples.

2 Experimental

2.1 Sample preparation

Thin free-standing films, thickness 90–486 μm, were prepared from polypropylene oxide based isocyanate terminated triol prepolymer, molecular weight of 6000 and each segment length of 10 nm; and polybutadiene diol, molecular weight of 2800 and chain length of 44 nm. The relative weight concentration of PU/PBDO studied is 60/40. The sample will be named PU60.

The preparation of PU and PBDO films was made according the procedure described in [8]. The two prepolymers were dissolved in toluene, under nitrogen atmosphere. For the reaction between the end groups, a drop of the catalyst dibutyl tin dilauryate (DBTDL) was added. Following a 30 min period, during which the reaction was allowed to proceed under stirring, the solutions were simultaneously cast and sheared by moving a calibrated Gardner Knife, at a controlled shear rate, 5 mm/s, onto a coated glass plate, at room temperature ($T \approx 25\,^{\circ}$C). After that, for curing, the film was placed in an oven at 70–80 °C for 3 h, it was exposed to air and continued curing for at least 72 h in atmospheric moisture.

Ferrofluid-doped samples were obtained by first preparing a mixture of ferrofluid (EMG911, from Ferrotec Corp.) with toluene that was left to homogenize for some minutes at room temperature under stirring. We used a surfacted ferrofluid (SFF), which consists of magnetite grains (Fe_3O_4, sample coated with an anionic surfactant) in a synthetic isoparaffinic solvent carrier. The anionic surfactant molecules present in the nanoparticle surface layer leave only the carbonic chain of them in contact with the elastomeric matrix. The reactive part of the molecule is attached to the nanoparticle. This process is essential to produce a stable magnetic colloid. So, no chemical reaction is expected to occur between the carbonic chain of the surfactant molecules around the nanoparticles and the elastomer. The particle diameter is about 10 nm (Ferrotec Corp. catalog information). Doped films of PU/PBDO elastomer (486 μm thick) were subsequently synthesized by adding the ferrofluid/toluene mixture to the prepolymers PU and PBDO at 60/40 relative wt%. After adding the catalyst, the experimental procedure was the same employed in the previous case of undoped samples. Visually, no agglomeration of grains was observed in the precursor solutions or in the films. By measuring the optical absorption coefficient, due mainly to the magnetic nanoparticles incorporated into the elastomeric matrix, we obtained the actual particles' concentrations in the samples that, in the present study were $c_{\mathrm{FF}} = 0.013$ vol% and 0.08 vol%, which correspond to 0.062 wt.% and 0.373 wt.%, respectively. These concentrations correspond to 2.5×10^{14} and 1.5×10^{15} particles per cm^3, respectively. For a homogeneous distribution of particles, these concentrations lead to a distance between two neighboring particles of about 200 nm and 110 nm, respectively. These samples will be hereafter named PU60f.

In the case of samples with oriented nanoparticles, after casting the films were subjected to the influence

of a magnetic field of about 100 Gauss, produced by Helmholtz coils, during the first 3 hours of the films curing at room temperature. After that, the film continued curing for at least 72 h in atmospheric moisture or placed in an oven at 70–80 °C for 3 h and left for at least 72 h in atmospheric moisture. It is expected that temperature in this case will only influence the kinetics of crosslinking reactions. Moreover, the samples were studied only after the crosslinking reaction is complete. We will come to this point later on.

In order to produce films with latent micro- and nanoperiodic patterns, some samples removed from the substrate, with and without ferrofluids, were exposed to ultraviolet light (UV, $\lambda = 254$ nm) for 3 days. Two different procedures were adopted, according to the literature [22], to develop the films and obtain textures with long corrugated, randomly distributed line-like patterns or textures with periodic modulation. In order to obtain free-standing films presenting the former texture, they were immersed in toluene in a soxhlet apparatus, during 36 h and dried in an oven at 70–80 °C for at least 72 h. The latter textures were observed after submitting the free-standing films to a uniaxial stress along the shear direction.

2.2 X-Ray Diffraction setup (NanoStar)

Elastomer samples are placed in a chamber, with a micrometric stretching device, positioned in the X-ray diffractometer (WAXS NanoStar from Bruker Instruments). The X-ray beam collimation system consists of 3 pinholes. The first pinhole (750 μm) is the divergence pinhole and the second pinhole (400 μm) is the beam-defining pinhole. Both, the divergence and the defining pinholes limit the maximum divergence of the "nearly" parallel beam. The third pinhole (1000 μm) is the anti-scatter pinhole, which shadows all edge scattering from the second pinhole. The collimated and monochromatic X-ray ($\lambda_x = 0.154$ nm) beam is oriented perpendicularly to the biggest elastomer film surface (z-axis of the laboratory frame). The voltage and current used in the X-ray tube generator are 40 kV and 30 mA, respectively. The experiments were done in the Laue geometry under vacuum. The diffractograms were registered in image plates and then digitalized and analyzed. The experimental resolution, obtained from the width at half-height of a Bragg peak from a single crystal, is $\sim 0.38 \pm 0.01$ degrees. This value was used to correct the measured width at half-height of the sample's diffraction peaks. The temperature of the experiment was fixed in 25 °C. The x-axis of the laboratory frame is defined by the stretching direction. The angle between the z-axis and the direction defined by the specimen's position and the diffraction point in the image plate is the scattering angle 2θ. The scattering vector modulus is defined as $s = (2\sin\theta)/\lambda_x$. The micrometric stretching device fix about 1 mm of the elastomeric film at both ends. The length L_0 is defined as the unstretched length of the sample and L is the length under stretching. The relative stretch is defined as $\varepsilon = \Delta L/L_0$, where $\Delta L = L - L_0$. The stretching direction coincides with that of the casting applied during the elastomer preparation. In the present study we were restricted to elastic domain with $\varepsilon \leq 0.25$.

2.3 Nuclear Magnetic Resonance setup

The proton spin-lattice relaxation times T_1 were obtained by using two different spectrometers, in order to cover a broad frequency range from 10 kHz to 100 MHz [23]. T_1 measurements at Larmor frequencies between 10 kHz and 4 MHz were performed in a home-developed fast field-cycling spectrometer [24], with a polarization and detection fields of 0.21 T (corresponding to the Larmor frequency of 8.9 MHz), and switching times of 2–3 ms. Standard fast field-cycling NMR techniques were used to measure the spin-lattice relaxation time [25,26].

The T_1 data between 4 and 100 MHz were obtained in a conventional pulsed NMR Bruker spectrometer with a 0–2.1 T electromagnet and an Avance II 300 console, using the inversion-recovery radio-frequency pulse-sequence with phase cycling $((\pi)_x - (\pi/2)_{x,-x})$ for suppression of the dc bias.

Both spectrometers offer the possibility to make angular-dependent measurements, since the samples can rotate perpendicularly to the Zeeman magnetic field.

The NMR samples consisted of a few rectangular samples of a few mm^2 stacked on the top of each other and fixed on the sample holder by both ends. The temperature was controlled within ± 0.5 °C. The magnetization (observed through the amplitude of the FID signals) showed mono-exponential time dependence evolution, suggesting that a uniform T_1 is established in the sample. The experimental error in the spin-lattice relaxation measurements is estimated to be less than $\pm 10\%$.

2.4 Mechanical setup

The mechanical properties of the samples were investigated by using an extensometer from Rheometric Scientific (Minimat Firmware version 3.1), at 25 °C. Rectangular, 10 mm × 5 mm (free surface, and $L_0 = 10$ mm), films samples were cut with their longest dimension either parallel or perpendicular to the casting shear direction. The film was stretched uniaxially at a rate of 2 mm/min, along the longest sample dimension (which is equal to L_0). The basic features of the stress/strain curves obtained are similar to those reported in the literature for this kind of network [8]. A mechanical property of a given sample was taken to be the average of the results of six successful measurements.

2.5 Optical, Atomic Force (AFM) and Magnetic Force (MFM) microscopy

Optical microphotograhs were taken in a Leitz polarizing microscope with parallel polarizers, in transmitted light geometry. Films undoped and doped with ferrofluids, after exposed to the UV light, were cut in slabs of 10 mm × 5 mm

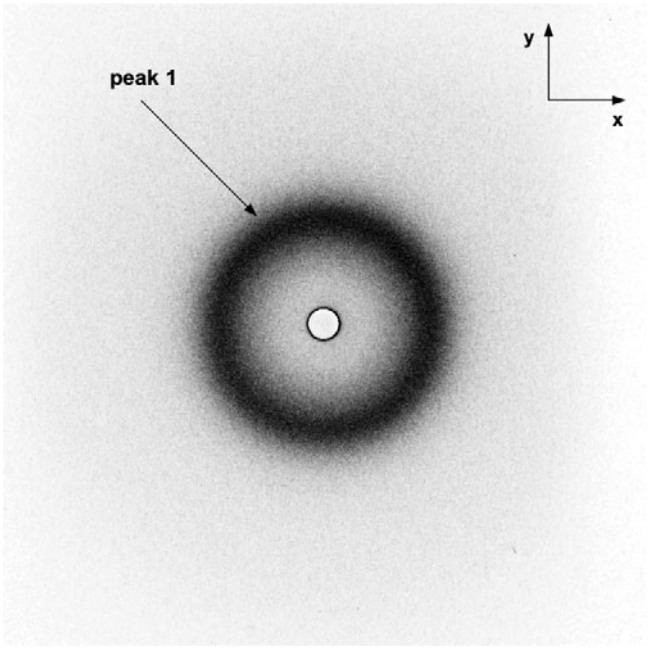

Fig. 1. Typical X-ray diffraction pattern of undoped sample PU60, unstretched. The characteristic peak is identified as peak 1.

(free surface), with the longest dimension of the sample along the casting shear direction. Films were stretched uniaxially with $\varepsilon = 0.43$ and left to relax as a function of time. Samples exposed to UV light and after extracted with toluene, but not stretched were also analyzed. The sample temperature was set to 25 °C. A Nanoscope IIIa multimode SPM apparatus from Digital Instruments was employed in the AFM and MFM observations. AFM measurements were performed in tapping mode and MFM in non-contact mode with a piezoelectric scanning. Measurements of the magnetic-force gradient distribution above the sample surface were also performed with the same apparatus. In addition to the capture of 3D images the surface mean roughness R_a and the root-mean-square roughness R_q can also be measured.

3 Results and discussion

3.1 The X-ray assays

The X-ray diffraction patterns of the undoped elastomers present a broad diffraction peak, almost isotropically disposed around the z-axis, as shown in fig. 1. This is consistent with the picture of an almost isotropic elastomeric matrix formed by the network of PU and PBDO molecules. This peak will be called hereafter peak 1. In fig. 2a the diffracted intensity is plotted as a function of s, along the y-direction. The characteristic distances associated to the peak were found to be $d_{1x} = 0.463 \pm 0.008$ nm and $d_{1y} = 0.459 \pm 0.008$ nm, almost independent of the stretching condition. We associate peak 1 with the distance between neighboring molecular segments in the elastomeric matrix. The correlation lengths (D_{1i}, $i = x, y$)

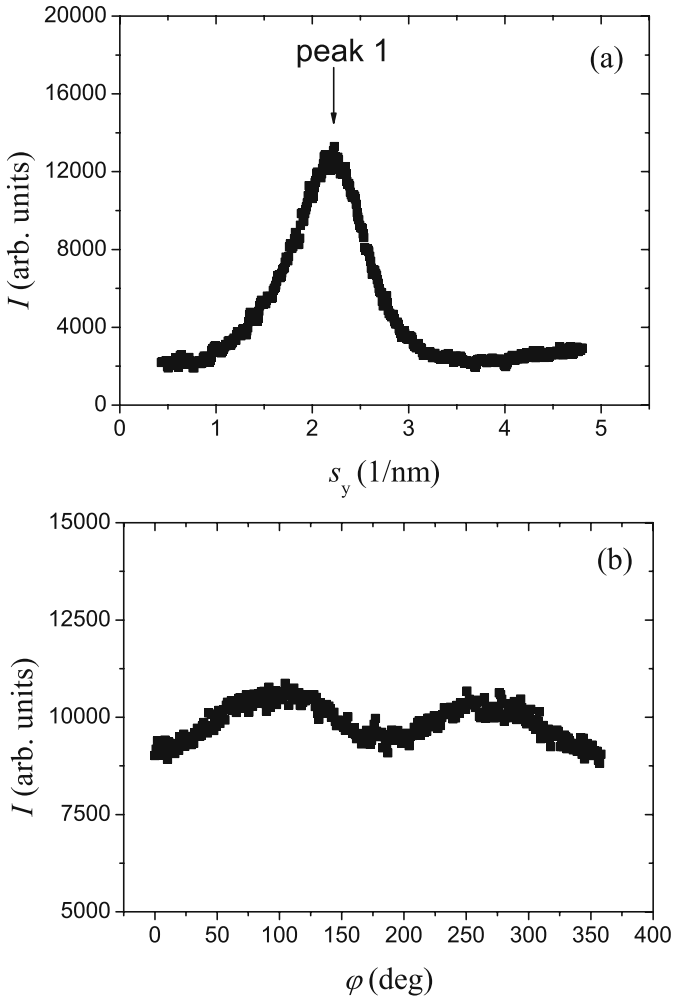

Fig. 2. Typical X-ray diffracted intensity of undoped sample PU60, unstretched. a) as a function of s, along the y-axis; b) as a function of the azimuthal angle φ.

were obtained from the widths at half-height of the peak, by using Scherrer's formula [27]. We observed that $D_1 \sim 1.1$ nm at $\varepsilon = 0$, remaining almost unchanged with the stretching, within our experimental accuracy. The correlation length obtained reveals that the typical ordering in the elastomeric matrix extends laterally to about 3 ($\sim D_1/d_1$) scatterers.

The diffracted intensities (I) along the x and y axes are slightly different, with $I_{1y}/I_{1x} \sim 1.10$ at $\varepsilon = 0$. The azimuthal angle analysis of the diffracted intensity (angle φ, measured in the xy plane, starting from the x-axis, in the counterclockwise direction) corroborates the conclusion that the peak intensity is higher along the y-axis (fig. 2b). The orientational order-parameter (OP) was obtained according to the Deutsch calculation [28], from the azimuthal diffracted intensity $I(\varphi)$ as

$$OP = 1 - N^{-1}\frac{3}{2}\int_0^{\pi/2} I(\varphi)\{\sin^2\varphi + (\sin\varphi)(\cos^2\varphi) \times \ln[(1+\sin\varphi)/\cos\varphi]\}\mathrm{d}\varphi, \quad (1)$$

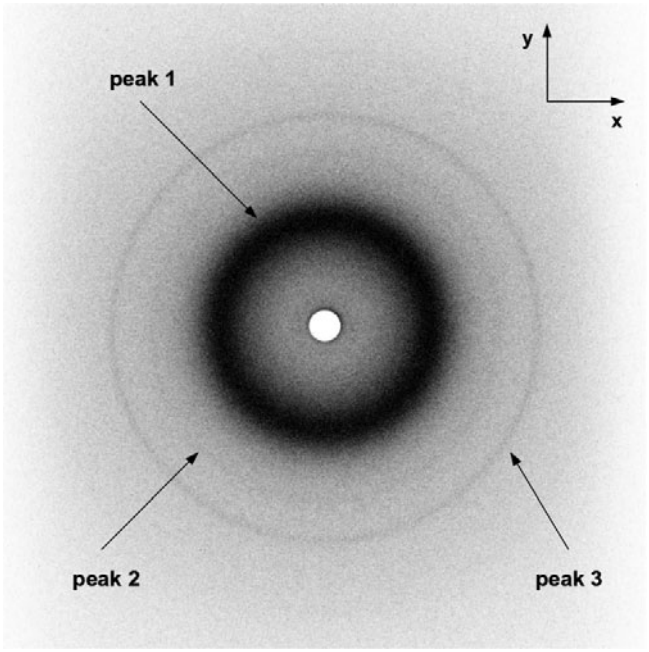

Fig. 3. Typical X-ray diffraction pattern of ferrofluid doped sample with $c_{\mathrm{FF}} = 0.08$ vol%, unstretched. The characteristic bands are identified as peak 1, 2 and 3.

where the zero angle in the integral refers to the equatorial position and the normalizing constant N is defined as

$$N = \int_0^{\pi/2} I(\varphi)\mathrm{d}\varphi.$$

The order parameter of the undoped sample, without any stress applied, was shown to be 0.16. This anisotropy observed in the film around the z-axis, under our experimental conditions, seems to be imposed by the casting. It is responsible for the optical anisotropy previously observed in unstretched elastomer films [5]. The stretching with $\varepsilon = 0.25$ imposed an increase of the orientational ordering to $OP = 0.25$. The picture of the structure of the elastomeric network under stretch, at this length scale, is particularly interesting. It is known that some macroscopic properties (*e.g.*, the birefringence) of this material change a lot when the elastomer is stretched [5]. However, the characteristic distance associated to the peak 1 and its correlation length is practically independent of the stretch condition, but the orientational order parameter increases as ε increases. In other words, the correlation volumes with typical dimension of about $(D_1)^3 \sim 1.5\,\mathrm{nm}^3$ remain about of the same size when the sample is stretched. The mean distance between molecules also remains the same, but the orientational molecular ordering inside the correlation volumes increases with the stretching. Moreover, the stretching seems to progressively orient the correlation volumes with their symmetry axis parallel to the stretching direction, giving rise to a macroscopic birefringence proportional to ε, as experimentally verified [6].

In the case of the samples doped with ferrofluid ($c_{\mathrm{FF}} \leq 0.08$ vol%) three diffraction peaks can be observed in fig. 3, one broad peak (peak 1) is due to the elastomer and the other two (named peaks 2 and 3) are associated to the ferrofluid particles present in the elastomeric matrix. They correspond to the [220] and [311] diffractions of the spinel-like structure of the Fe_3O_4 particles [29], with lattice parameter of 0.8379 nm. The values of d_{1y}, D_{1y} and d_{1x}, D_{1x} remain, within the experimental errors, comparable to those from the undoped samples, practically independent of ε and the amount of nanoparticles. The peak transmittance is also more intense along the y-axis direction: $I_{1y}/I_{1x} \sim 1.10$ at $\varepsilon = 0$. The azimuthal angle analysis of the diffracted intensity allowed the calculation of the orientational order parameter using eq. (1). The values of the OP obtained in both nanoparticles doping conditions were of the order of 0.22, and practically independent of the stretching conditions. This observed difference with respect to the value of the OP of the undoped elastomer is small but clearly larger than the experimental uncertainty.

The fact we did not observe any significant modification in the values of d_{1y}, D_{1y} and d_{1x}, D_{1x} from doped samples, with respect to those from undoped samples, indicates that the elastomeric structure is practically unchanged (or slightly modified but undetected by our experimental diffraction method) by the presence of the magnetic nanoparticles. However, the orientational order parameter, even in the unstretched condition, is higher (about 35%) when compared to that of undoped samples. This result could explain why we measured [5] a higher value of the optical birefringence in a nanoparticle doped elastomer when compared to the undoped sample, even at $\varepsilon = 0$.

The dark intense apparent ring visible at low angles (around the hole in the imaging plate sheet) in fig. 1 is due to the small-angle scattering produced by large correlation lengths present in the sample. It is highly improbable that phase separation occurs at this length scale. Moreover, this scattering is no more visible in the sample doped with ferrofluid. These correlation lengths may be due to an electronic modulation of the structure in large scale, which is lost after the introduction of the nanoparticles in the matrix. The interpretation of these contributions is beyond the scope of this article and will be investigated in the future.

3.2 The NMR assays

Figure 4 shows the ^{1}H spin-lattice relaxation time (T_1) as a function of the Larmor frequency (ν_{L}) of the PU60 undoped and PU60f doped with ferrofluid ($c_{\mathrm{FF}} = 0.013$ vol%). The temperature of the sample was set at 85 °C to improve the signal-to-noise ratio in the spectrometer. At room temperature the values of T_1 at low frequencies are close to the detection limit of our equipment. We experimentally verified for the undoped sample (data not shown) that the shapes of the dispersion curves at room temperature (T_1 *versus* ν_{L}) are identical to those at 85 °C, only shifted towards higher values of T_1 for increasing temperatures.

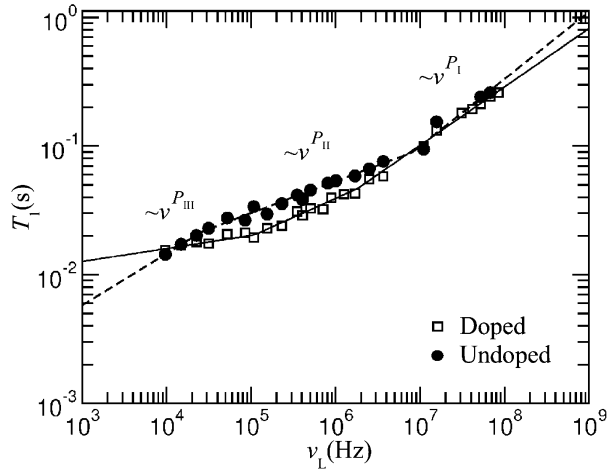

Fig. 4. Spin-lattice relaxation time (T_1) as a function of the Larmor frequency (ν_L) of the undoped PU60 sample (•) and ferrofluid-doped PU60f sample with $c_{FF} = 0.013$ vol% (□). The solid and dashed lines are best fits of the renormalized Rouse model performed. Fitting parameters (P_j with $j = I, II, III$) of the power law dependence of T_1 as a function of the Larmor frequency ($T_1 \propto \nu_L^{P_j}$) and cut-off frequencies (f) of the undoped sample: $P_I = 0.52 \pm 0.01$, $P_{II} = 0.25 \pm 0.01$, $P_{III} = 0.40 \pm 0.17$, $f_{I\text{-}II} = 85 \pm 1 \times 10^5$ Hz, $f_{II\text{-}III} = 2.8 \pm 0.01 \times 10^4$ Hz; of the doped sample: $P_I = 0.45 \pm 0.02$, $P_{II} = 0.30 \pm 0.03$, $P_{III} = 0.10 \pm 0.03$, $f_{I\text{-}II} = 18 \pm 9 \times 10^5$ Hz, $f_{II\text{-}III} = 11 \pm 1 \times 10^4$ Hz.

A spin-lattice relaxation time increase with (increasing) frequency is observed in all frequency regions for the two undoped and doped ($c_{FF} = 0.013$ vol%) systems, both at 85 °C and at room temperatures.

In the case of undoped samples, three linear regions can be identified and may be described in the framework of the renormalized Rouse model for the molecular dynamics of the elastomer constituents [30]. In this model $T_1 \propto (\nu_L)^{P_j}$, with j referring to the particular Larmor frequency range. The processes occurring in the first and second regions of the dispersion curves depicted in fig. 4 ($\nu_L \gtrsim 10^7$ Hz, region I; 2.5×10^4 Hz $\lesssim \nu_L \lesssim 10^7$ Hz, region II) refer to dipolar intra-segment interactions. In the third region of the dispersion curve ($\nu_L \lesssim 2.5 \times 10^4$ Hz, region III) the processes refer to dipolar inter-segments interactions. The fitting parameters obtained with the Rouse power law in the different regions are given in the caption of fig. 4. The values of the exponents for the undoped PU60 system are quite similar to others reported in the literature for other polymers [21].

The ferrofluid-doped sample ($c_{FF} = 0.013$ vol%) presented systematically smaller T_1 values than those obtained in undoped samples in the frequency range of 2×10^4 Hz to about 10^7 Hz. The same experiment performed with magnetic grains oriented in the elastomeric matrix (by applying a magnetic field during the sample synthesis, and prepared according to both methods described in the Experimental section) gave the same results of unoriented particles. The fact that the behavior of T_1 as a function of ν_L is the same for samples prepared with and without the period spent in the oven reinforces the idea that temperature only influences the kinetics of crosslinking reactions. In the case of the doped PU60f film the values of the fitted exponents P_I and P_{II} are still within the range usually associated with the intra-segment relaxation contributions, although P_I is slightly smaller than that obtained for the undoped film. In the low-frequency domain the exponent P_{III} is quite different from the value obtained in the undoped film. According to the renormalized Rouse relaxation model for polymers, the relaxation observed at low frequencies is usually associated to inter-segment relaxation contributions. Therefore, the presence of the nanoparticles in the elastomer seems to strongly influence the relaxation contribution associated with these interactions. These results indicate that the presence of the doping particles affects the local ordering of the elastomer network in the neighborhood of them. As the values of P_I and P_{II} are quite similar in the undoped and doped ($c_{FF} = 0.013$ vol%) systems, we can conclude that the intra-segment relaxation contributions are less affected by these changes in the local ordering.

At higher magnetic nanoparticles concentrations the dispersion curve could not be obtained in our experimental setups. For $c_{FF} = 0.08$ vol% PU60f system the larger concentration of magnetic nanoparticles dispersed in the elastomer film strongly reduces the homogeneity of the magnetic field in the measuring volume, thus shortening the detected FID signal. Some values of T_1 from the $c_{FF} = 0.08$ vol% PU60f system were measured at high frequencies (between 31 MHz and 85 MHz), at the temperatures of 25 °C and 85 °C. The values of T_1 obtained in both temperatures were similar (within our experimental uncertainty) to those obtained for the doped $c_{FF} = 0.013$ vol% system. This indicates that the intra-segment relaxation contributions are similar in both nanoparticles concentrations. One should expect more important changes in the relaxation in the low-frequency range (inter-segment coupling). An increased ordering induced by the larger number of nanoparticles is detected by X-rays diffraction. However, measurements at lower frequencies were not possible due to technical limitations of the fast field-cycling NMR spectrometer used.

3.3 The mechanical assays

Table 1 shows the values of the Young modulus (E), stress and strain at break and toughness of the samples in different experimental situations. The symbols $\parallel$ and $\perp$ refer to the configuration parallel and perpendicular to the casting direction, respectively. Let us first analyze the undoped sample. The value of E when the stretching direction is parallel to the casting direction ($E_\parallel$) is about 3% bigger than the value when the stretching direction is perpendicular to the casting direction ($E_\perp$), in accordance with data obtained before for this kind of elastomers [8]. So, the casting introduces an orientation of the stick-like molecules with respect to the casting direction, detected in the optical birefringence at $\varepsilon = 0$ [6] and Young moduli experiments ([22] and table 1).

Table 1. Young modulus (E), strain (ε_b) and stress at break and toughness of the different assays performed. c_{FF} is the concentration of magnetic particles incorporated into the elastomer in volume %. The geometry of the different assays is also presented: C and H represent the directions of the casting and the magnetic field, respectively; the symbols $\parallel$ and $\perp$ refer to the assay parallel or perpendicular to the casting direction.

c_{FF} (vol%)	Assay orientation with respect to casting		Young modulus (10^{-3} MPa)	Strain at break (ε_b)	Stress at break (10^{-3} MPa)	Toughness (10^{-3} MPa)
0	$\parallel$	-	1809 ± 19	1.12	1212 ± 10	749 ± 5
	$\perp$	-	1764 ± 9	0.37	562 ± 5	105 ± 5
0.013	$\parallel$	-	1733 ± 14	2.14	1312 ± 10	1838 ± 10
	$\perp$	-	1583 ± 9	2.32	1191 ± 10	1911 ± 10
	$\parallel$	$H \parallel C$	1759 ± 9	1.86	1351 ± 10	1552 ± 10
	$\perp$	$H \parallel C$	1688 ± 12	1.48	1199 ± 10	1001 ± 5
	$\parallel$	$H \parallel C$	1656 ± 8	1.75	1309 ± 10	1347 ± 10
	$\perp$	$H \parallel C$	1585 ± 7	2.02	1295 ± 10	1634 ± 10
0.08	$\parallel$	-	1527 ± 80	1.97	1301 ± 10	1524 ± 10
	$\perp$	-	1527 ± 102	1.92	1339 ± 10	1612 ± 10
	$\parallel$	$H \parallel C$	1226 ± 102	1.92	1100 ± 10	1672 ± 10
	$\perp$	$H \parallel C$	1504 ± 365	1.36	1038 ± 10	1140 ± 10

When the magnetic particles are incorporated into the elastomeric matrix (particles not oriented by any external magnetic field ($c_{FF} = 0.013$ vol% and 0.08 vol%)), both moduli ($E_\parallel$, $E_\perp$), decrease with respect to those from undoped samples. In this case $E_\parallel$ is about 9.5% bigger than $E_\perp$. Comparing the Young moduli $E_\parallel$ and $E_\perp$ in the situations where the magnetic particles are oriented by an external magnetic field when incorporated into the elastomeric matrices, we note that: i) the presence of magnetic nanoparticles with their magnetic moments (μ) parallel to the casting and stretching direction increases (by about 6%) the value of $E_\parallel$ with respect to that obtained when the particles were oriented with their magnetic moment perpendicular to the casting and stretching direction (μ perpendicular to the biggest surface of the film); ii) the presence of magnetic nanoparticles with their magnetic moments (μ) perpendicular to the casting and stretching direction (μ perpendicular to the biggest surface of the film) decreases (by about 6%) the value of $E_\perp$ with respect to that obtained when the particles were oriented with their magnetic moment parallel to the casting and perpendicular to the stretching direction (μ parallel to the biggest surface of the film). Also here we did not see any measurable difference between the samples which stayed or not in the oven during the sample preparation. In general, the Young moduli of samples without the magnetic nanoparticles are bigger than those obtained from ferrofluid-doped samples.

The differences in the values of E obtained with both nanoparticles' concentrations investigated are small but show a clear trend. In all the cases, the Young modulus measured in the geometry parallel ($\parallel$) to the casting direction is larger than that measured in the perpendicular ($\perp$) condition. The relative decrease of $E_\parallel$ and $E_\perp$, measured in doped films with respect to those obtained in the undoped samples, is of the order of 4% and 12%, respectively. The orientation of the magnetic moments of the particles during the elastomer preparation contributes slightly to modify the values of E with respect to those obtained with unoriented magnetic moments. The presence of the ferrofluid particles (oriented or not) in the elastomeric matrix seems to soften the structure, in particular, in the direction perpendicular to the casting direction. The ferrofluid particles may act like defects in the previously homogeneous elastomeric structure. These defects could be responsible for the unusual decreasing of E in samples doped with ferroparticles.

The strain and stress at break and the toughness of doped samples are bigger than those obtained with the undoped samples. These results indicate that the presence of the nanoparticles in the elastomer makes it more resistant to the rupture when subjected to a strain. The increase in particles concentration, at least in the investigated range, did not improve this resistance of the doped samples. An interesting result can be observed when we compare the values of the toughness of the doped samples prepared in the presence of the magnetic field (regardless of the fact that the sample has been in the oven during its preparation). A decrease of the value of this parameter is observed in samples prepared with the field with respect to those obtained in doped samples prepared without the field. An effect of the magnetic field applied during the sample preparation is the formation of micron-size clusters (we will discuss this aspect in the following), formed

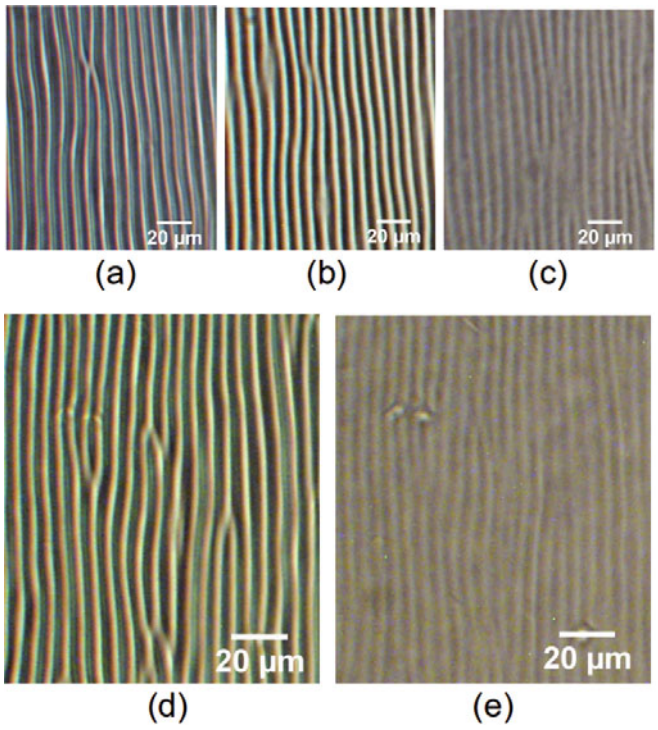

Fig. 5. Optical microscopy observation of textures of films exposed to UV light, stretched with $\varepsilon = 0.43$ and after left to relax. Stretching parallel to the casting direction. Stripes perpendicular to the casting direction. Undoped film starting to relax (a); after 75 min (b); after 19 h 30 min (c). Doped film starting to relax (d); after 75 min (e).

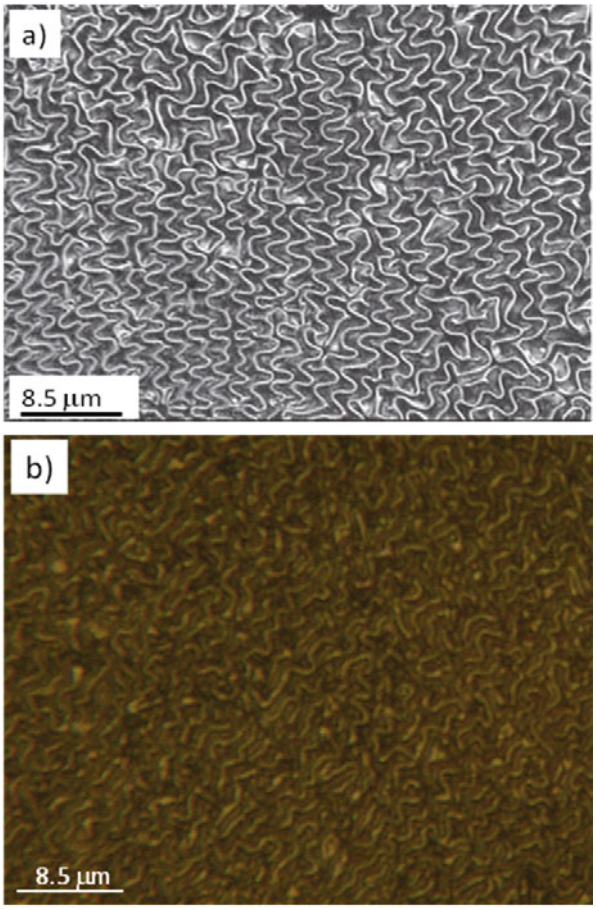

Fig. 6. Optical microscopy observation of toluene extraction performed with a) undoped film, and b) nanoparticles-doped film.

by aggregated nanoparticles. The result of this process is the migration of nanoparticles from the bulk (more homogeneous distribution) to the clusters.

3.4 The Optical Microscopy, AFM and MFM assays

It is known that undoped elastomer films exposed to UV radiation can, under certain stretching conditions, develop periodical bands on their surfaces. These patterns vanish after some time, depending on the sample mechanical treatment and UV exposure time. Figures 5a, b and c show the optical microscopy texture of the undoped film exposed by 27 h to the UV light, after stretching with $\varepsilon = 0.43$ and left to relax as a function of time. The stretching was applied parallel to the casting direction and the stripes are perpendicular to the stretching direction. Figures 5a, b and c were obtained at $t = 0$ (start of the relaxation process), $t = 75$ min and $t = 19$ h 30 min, respectively. The distance between consecutive bands observed remains the same as a function of time ($7.5 \pm 0.6\,\mu$m), however, this texture vanishes after some days. The toluene extraction performed with undoped films showed the typical micron-sized pattern shown in fig. 6a. The pattern is composed by well-defined stripes almost regularly spaced on average (typical distance between stripes of about $1.6\,\mu$m). This pattern remains unchanged as a function of time.

The doped ($c_{\mathrm{FF}} = 0.013$ vol%) irradiated sample was subjected to a (elastic) uniaxial deformation ($\varepsilon = 0.43$) along shear rate direction. After removal of this stress a periodic pattern ("bands") developed on the elastomer film surface with wave vector parallel to the shear direction. The optical microscopy texture observed under parallel polarizers, obtained with the microscope focused near the surface, can be observed in fig. 5d. The textures observed for the undoped film, subject to the same treatment, can be observed in fig. 5a. It was reported in the literature [22] that these states decay with a time constant that is a function of the rate of extension which was used to produce them. Figures 5d and e were obtained at $t = 0$ (start of the relaxation process) and $t = 75$ min, respectively. The distance between consecutive bands observed remains the same as a function of time ($5.7 \pm 0.5\,\mu$m). In the case of doped samples we found that, for the same experimental conditions, the bands disappear more rapidly than for the undoped films. The mechanism that is thought to be responsible for the development of the bands is the formation of a stiff layer at the top of the film, induced by UV light. This layer has different mechanical properties from the rest of the film. This top layer corresponds to a "harder" material which most

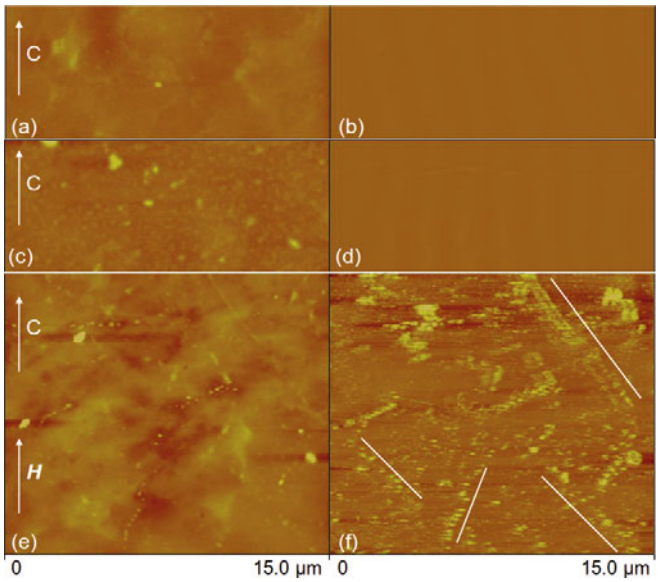

Fig. 7. AFM and MFM pictures of the samples in different experimental conditions. Each pair a-b, c-d, e-f represents the AFM-MFM picture of the same sample region. Undoped sample: panels a and b; doped sample with $c_{\mathrm{FF}} = 0.013$ vol%, prepared without the magnetic field: panels c and d; doped sample with $c_{\mathrm{FF}} = 0.013$ vol%, prepared with the magnetic field ($\boldsymbol{H}$) applied parallel to the casting direction (C): panels e and f. The lines in panel f are only guide for the eyes indicating the direction of linear aggregates.

probably results from cross-linking due to the presence of PBDO double bonds and oxigen, under the catalytic action of UV light. The surface textures of doped samples disappeared earlier than for the undoped sample, which can be due to the different viscoelastic flow properties of the plastically deformed state. Those results are in accordance with the mechanical measurements for doped and undoped samples. The texture of extracted doped ($c_{\mathrm{FF}} = 0.08$ vol%) elastomers in toluene and drying conditions exhibits micron-sized features along all axes (fig. 6b), as already observed for undoped samples [22], revealing a more diffuse pattern. The spacing between surface features is about 2.0 μm. This pattern, similarly to undoped films, also remains unchanged as a function of time indicating that, for the exposure time used (3 days), the oxidative cross-linking occurs in the presence of the nanoparticles.

The AFM and MFM pictures of the samples in different experimental conditions are presented in figs. 7 and 8. The casting direction is represented by the arrow and the label C. The pairs a-b, c-d and e-f represent the AFM-MFM pictures of the same region of the samples. Figures 7a and b show the aspect of the undoped elastomer sample. Figures 7c and d show the doped samples ($c_{\mathrm{FF}} = 0.013$ vol%) prepared without the magnetic field. Figure 7d is compatible with a picture of a homogeneous distribution of magnetic nanoparticles dispersed in the elastomeric matrix. The resolution of the MFM setup does not allow us to see particles in the scale of tens of nanometers. Figures 7e and f show the AFM and MFM picture of the doped ($c_{\mathrm{FF}} = 0.013$ vol%) sample prepared with the

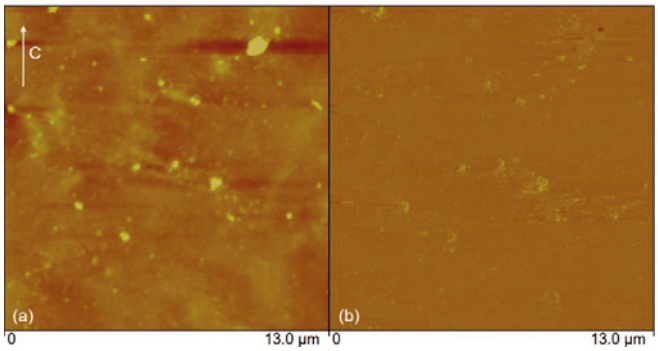

Fig. 8. AFM (a) and MFM (b) pictures of doped sample with $c_{\mathrm{FF}} = 0.08$ vol%, prepared without the magnetic field. The label C indicates the casting direction.

magnetic field (label $\boldsymbol{H}$) parallel to the casting direction. Now big aggregates, some of them of linear shape, are visible mainly in the MFM picture (regardless of the fact that the sample has been in the oven during its preparation). These linear aggregates present a mean orientation along the field direction. The characteristic dimensions of these aggregates are presented in table 2. We observed in some regions of the same sample a picture like that of fig. 7d, indicating that there are regions where the particles are still not aggregated and/or they were removed to form the aggregates in other sample regions. Figures 8a and b show the pictures of the doped sample ($c_{\mathrm{FF}} = 0.08$ vol%) prepared without the magnetic field. The MFM picture (fig. 8b) shows the presence of magnetic aggregates in the sample, whose characteristic dimensions are presented in table 2. Our results indicate that bigger aggregates are obtained when the magnetic field is applied during the preparation process, regardless of the magnetic particles concentration of the sample, at least in the concentration range investigated. Our MFM results seems to indicate that some of the almost linear magnetic particle aggregates do not orient completely parallel to the field because of the high viscosity of the fluid during the casting process (the cross-linking process has taken place) and also because the magnetic field from the Helmholtz coils employed is rather low. The field was not increased to avoid the spurious heating of the film during the casting.

Undoped and doped samples shows the same surface mean roughness $R_a \sim 2$ nm and the root-mean-square roughness $R_q \sim 2.74$ nm (undoped sample), 3.46 nm (doped with $c_{\mathrm{FF}} = 0.013$ vol% prepared without the magnetic field), 4.11 nm (doped with $c_{\mathrm{FF}} = 0.013$ vol% prepared with the magnetic field) and 4.92 nm (doped with $c_{\mathrm{FF}} = 0.08$ vol% prepared without the magnetic field).

4 Conclusions

The structures of the elastomers of PU/PBDO without and with ferromagnetic nanoparticles incorporated were studied by using the X-ray diffraction, AFM, MFM, mechanical assays and nuclear magnetic resonance techniques. The structure proposed for the pure elastomer

Table 2. Statistical data from the magnetic particles aggregates observed in fig. 7f, doped sample with $c_{FF} = 0.013$ vol%, prepared with the magnetic field parallel to the casting direction; and fig. 8b, doped sample with $c_{FF} = 0.08$ vol%, prepared without the magnetic field.

c_{FF} (vol%)	Mean value (μm)	Standard deviation (μm)	Minimum value (μm)	Maximum value (μm)	Variance (μm^2)	Coefficient of variance
0.013 (with H)	0.136	0.169	0.042	1.741	0.028	1.241
0.08	0.105	0.090	0.036	0.721	0.008	0.857

is that of a molecular network (*i.e.*, a cross-linked polymer network) where the characteristic distance between cross-linked parallel molecular segments is of the order of 0.46 nm. The correlation length (D) obtained is of the order of 1.15 nm. The casting performed in the experimental procedure to obtain the elastomeric films introduces anisotropy in the network, tending to orient the stick-like chains between cross-links parallel to the casting direction. Under stretch ($\varepsilon \leq 0.25$), the characteristic distance between molecules and the correlation distance are independent of the stretch, but the orientational order parameter increases with the stretch.

In the case of nanoparticles-doped samples the elastomeric structure probed by the X-ray experiments is similar to the one observed for the undoped films. Nevertheless, the casting-induced order parameter was shown to be about 35% larger than the one obtained for undoped samples. NMR experiments also evidence modifications in the network local ordering in nanoparticles doped elastomers. The presence of nanoparticles in the structure weakens the dependence of T_1 on the Larmor frequency in the inter-segment interactions region of the dispersion curve. On the other hand, since the values of $P_{\rm I}$ and $P_{\rm II}$ are similar in both undoped and doped ($c_{FF} = 0.013$ vol%) systems, we can conclude that the intra-segment relaxation contributions are less affected by the changes in the local ordering imposed by the particles encrusted in the elastomeric network.

The films mechanical behavior was found to be influenced by the presence of a small amount of nanoparticles used. The undoped films were found more brittle than the doped samples. The orientation of the magnetic moments of the particles during the elastomer preparation contributes slightly to modify the values of E with respect to those obtained with unoriented magnetic moments. But, the presence of the ferrofluid particles (oriented or not) in the elastomeric matrix seems to soften the structure, in particular, in the direction perpendicular to the casting direction. The values of the toughness of the doped samples prepared in the presence of the magnetic field decrease with respect to those obtained in doped samples prepared without the field. The MFM experiments revealed that even in magnetic particles' concentrations as small as 0.08 vol% (without any field applied during the sample preparation) particles aggregate in clusters of micrometer dimension. On the other hand, at smaller particles concentration, aggregates were observed only when the magnetic field was applied during the sample preparation. The ferrofluid particles may act like defects in the previously homogeneous elastomeric structure.

Those mechanical characteristics can be responsible for the relaxation behavior of patterns observed on UV irradiated samples. In the case of doped samples the bands disappear more rapidly than for the undoped films. The texture of the extracted doped elastomers in toluene and drying conditions also remains unchanged as a function of time, similarly to undoped films, indicating that the oxidative cross-linking occurs in the presence of the nanoparticles.

The authors thank CNPq, FAPESP, CAPES/GRICES-175/07, and INCT-FCx (Instituto Nacional de Ciência e Tecnologia de Fluidos Complexos) for financial support. This work was partially supported by PTDC/CTM/099595/2008 and by Portuguese Science Foundation (FCT) through Pluriannual Contracts with CENIMAT/I3N. P. J. Sebastião and D. Sousa thank J. Cascais for the technical help in the development of the new FFC NMR spectrometer. We thank Prof. C.L.P. de Oliveira for helpful discussions.

References

1. C.T. Zhao, M.N. de Pinho, Polymer **40**, 6089 (1999).
2. D.P. Queiroz, M.C. Gonçalves, M.N. de Pinho, J. Appl. Polym. Sci. **103**, 315 (2007).
3. M.H. Godinho, J.L. Figueirinhas, C.T. Zhao, M.N. de Pinho, Macromolecules **33**, 7675 (2000).
4. M.H. Godinho, A.C. Trindade, J.L. Figueirinhas, L.V. Melo, P. Brogueira, Mol. Cryst. Liq. Cryst. **437**, 53[1297] (2005).
5. A.M. Figueiredo Neto, M.H. Godinho, T. Toth-Katona, P. Palffy-Muhoray, Braz. J. Phys. **35**, 184 (2005).
6. C. Sena, C. Bayley, M.H. Godinho, J.L. Figueirinhas, P. Palffy-Muhoray, A.M. Figueiredo Neto, J. Magn. & Magn. Mater. **300**, 79 (2006).
7. C. Sena, M.H. Godinho, A.M. Figueiredo Neto, J. Appl. Phys. **102**, 073524 (2007).
8. A.C. Trindade, M.H. Godinho, J.L. Figueirinhas, Polymer **45**, 5551 (2004).
9. A. Taborda, N. Louro, P.J. Sebastião, J.L. Figueirinhas, M.H. Godinho, Mol. Cryst. Liq. Cryst. **450**, 119[319] (2006).
10. M. Zrínyi, L. Barsi, A. Büki, J. Chem. Phys. **104**, 8750 (1996).

11. Z. Varga, G. Filipcsei, M. Zrínyi, Polymer **47**, 227 (2006).
12. M. Zrínyi, L. Barsi, A. Büki, Polym. Gels Networks **5**, 415 (1997).
13. Z. Varga, J. Fehér, G. Filipcsei, M. Zrínyi, Macromol. Symp. **200**, 93 (2003).
14. F. Bentivegna, M. Nyvlt, J. Ferré, J.P. Jamet, A. Brun, S. Visnovsky, R. Urban, J. Appl. Phys. **85**, 2270 (1999).
15. S. Bohlius, H.R. Brand, H. Pleiner, Phys. Rev. E **70**, 061411 (2004).
16. R. Fuhrer, E.K. Athanassiou, N.A. Luechinger, W.J. Stark, Small **5**, 383 (2009).
17. K.J. Suthar, M.K. Ghantasala, D.C. Mancini, J. Ilavsky, Proc. SPIE **7289**, 72891D (2009).
18. V.T. Lebedev, Gy. Torok, L. Cser, A.L. Buyanov, L.G. Revelskaya, D.N. Orlova, A.I. Sibiliev, J. Magn. & Magn. Mater. **201**, 136 (1999).
19. M. Ashjari, A.R. Mahdavian, N.G. Ebrahimi, Y. Mosleh, J. Inorg. Organomet. Polym. **20**, 213 (2010).
20. A. Sánchez-Ferrer, M. Reufer, R. Mezzengal, P. Schurtenberger, H. Dietsch, Nanotechnology **21**, 185603 (2010).
21. S. Ran, D. Fang, I. Sics, S. Toki, B.S. Hsiao, B. Chu, Rev. Sci. Instrum. **74**, 3087 (2003).
22. M.H. Godinho, A.C. Trindade, J.L. Figueirinhas, L.V. Melo, P. Brogueira, A.M. Deus, P.I.C. Teixeira, Eur. Phys. J. E **21**, 319 (2006).
23. A. Abragam, *The Principles of Nuclear Magnetism* (Clarendon Press, Oxford, 1961).
24. D.M. Sousa, G.D. Marques, J.M. Cascais, J.P. Sebastião, Solid State Nucl. Magn. Reson. **38**, 36 (2010).
25. F. Noack, Prog. Nucl. Magn. Reson. Spectrosc. **18**, 171 (1986).
26. R. Kimmich, E. Anoardo, Prog. Nucl. Magn. Reson. Spectrosc. **44**, 257 (2004).
27. B.D. Cullity, *Elements of X-Ray Diffraction*, second edition (Addison-Wesley Publ. Co. Inc. USA, 1978).
28. M. Deutsch, Phys. Rev. A **44**, 8264 (1991).
29. M. Ma, Y. Zhang, W. Yu, H. Shen, H. Zhang, N. Gu, Colloids Surf. A: Physicochem. Eng. Aspects **212**, 219 (2003).
30. N. Fatkullin, R. Kimmich, J. Chem. Phys. **101**, 822 (1994).